

The integral under consideration, therefore, is

$$\lim_{r \rightarrow \infty} \left( \frac{i\mu}{\hbar^2} \right) \int_0^{\infty} \frac{e^{-i\theta_\lambda} - \eta_\lambda e^{i\theta_\lambda}}{k_0^2 + i\epsilon - k^2} dk. \quad (28)$$

The two terms of this integral may be studied in the complex plane, by suitably closing and deforming the path of integration, initially along the positive real axis. Figure 3 shows how the closed paths must be chosen, encircling the first and fourth quadrants. For sufficiently large  $r$  the portions of path along the imaginary  $k$  axis and along the circle at infinity do not contribute, provided the lower path is used for the term  $\exp(-i\theta_\lambda)$  and the upper path for  $\exp(i\theta_\lambda)$ . Then only the second term leads to a nonvanishing residue

from the one pole at  $k = k_0 + i\epsilon$ . We find

$$\lim_{r \rightarrow \infty} \left( \frac{2\mu}{\hbar^2} \right) \int_0^{\infty} \frac{f_\lambda(k, r) dk}{k_0^2 + i\epsilon - k^2} = \left( \frac{2\mu}{\hbar^2} \right)^{\frac{1}{2}} i \left( -\frac{2\pi i}{2k_0} \right) (-\eta_\lambda e^{i\theta_\lambda(k_0)}).$$

The asymptotic Green's function, therefore, is

$$(E + i\epsilon - H_0)^{-1} \sim - (2\mu/\hbar^2) \exp[k_0 r - n \ln(2k_0 r)] / k_0 r r' \\ \times \sum_{\lambda\nu} e^{i(\sigma_\lambda - \frac{1}{2}\lambda\pi)} f_\lambda(k_0, r') Y_{\lambda\nu}(\Omega) Y_{\lambda\nu}^*(\Omega').$$

In the second line of this expression we recognize the familiar "time-reversed final-state wave function," denoted in the present article by  $\chi_f^{(-)*}$ . The above discussion is interesting in that it shows the origins of the various factors of the familiar expression and, in particular, the manner in which the Coulomb phase factor enters this expression.

## Effect of the Optical Potential on the Nucleon Momentum Distribution in Nuclei. The Pickup Reaction\*

PAUL A. BENIOFF

Argonne National Laboratory, Argonne, Illinois

(Received June 6, 1962)

The effect of the optical potential on the nucleon momentum distribution in nuclei is discussed in this work. The idea of McCarthy *et al.*, that the refraction and localization effects caused by the real and imaginary parts of the optical potential smears the single-particle momentum distribution, is amplified and applied to nucleon momentum distribution experiments. The assertion is made here that it seems impossible to directly measure in any manner the momentum distribution of nucleons in nuclei. Further it is proposed that much or all of the large discrepancy between the experimental momentum determinations and the shell-model predictions is due to the neglect of these important sources of high-momentum components. The high-energy  $C^{12}(p, d)C^{11}$  pickup reaction data are re-analyzed in the light of these considerations. It is shown that for  $q^2/\beta^2 \leq 8$ , the  $1p$ -shell harmonic oscillator distribution,  $(q^2/\beta^2) \exp(-q^2/\beta^2)$ , has sufficient high-momentum components to fit the data. The lack of agreement for  $q^2/\beta^2 > 8$  is possibly due more to a failure in the distorted-wave approximation calculation used here than to lack of high-momentum components in the wave function.

### I. INTRODUCTION

THE success of the shell model for predictions of various properties of nuclei such as energy levels, magnetic moments, etc., has been amply verified by many workers. However, it has not been so successful in predicting the momentum distribution of ground-state nucleons in target nuclei as found by various nuclear reaction studies.<sup>1-18</sup> In general, the experimental

results require much larger amounts, by orders of magnitude, of high-momentum components in the single-particle ground-state wave function than are supplied by the shell-model wave functions. This

\* Based on work performed under the auspices of the U. S. Atomic Energy Commission.

<sup>1</sup> O. Chamberlain and E. Segrè, *Phys. Rev.* **87**, 81 (1952).

<sup>2</sup> J. Cladis, W. Hess, and B. Moyer, *Phys. Rev.* **87**, 425 (1952).

<sup>3</sup> J. Wilcox and B. Moyer, *Phys. Rev.* **99**, 875 (1955).

<sup>4</sup> L. Azhgirev, I. Vzorov, V. Zrelov, M. Mescheryakov, B. Neganov, R. Ryndin, and A. Shabudin, *Nuclear Phys.* **13**, 258 (1958).

<sup>5</sup> J. McEwen, W. Gibson, and P. Duke, *Phil. Mag.* **2**, 231 (1957).

<sup>6</sup> J. Garron, J. Jacmart, M. Riou, and Ch. Ruhla, *J. phys. radium* **22**, 622 (1961).

<sup>7</sup> B. Gottschalk and K. Strauch, *Phys. Rev.* **120**, 1005 (1960).

<sup>8</sup> E. Henley, *Phys. Rev.* **85**, 204 (1952); C. Richman and H. Wilcox, *ibid.* **104**, 1710 (1956).

<sup>9</sup> M. Block, S. Passman, and W. Havens, *Phys. Rev.* **88**, 1239 (1952).

<sup>10</sup> M. Lax and H. Feshbach, *Phys. Rev.* **81**, 189 (1951).

<sup>11</sup> G. Chew and M. Goldberger, *Phys. Rev.* **77**, 470 (1950).

<sup>12</sup> A. Wattenberg, A. Odian, P. Stein, H. Wilson, and R. Weinstein, *Phys. Rev.* **104**, 1710 (1956).

<sup>13</sup> W. Selove, *Phys. Rev.* **101**, 231 (1956).

<sup>14</sup> H. Hagiwara and M. Tanifugi, *Progr. Theoret. Phys.* **18**, 97 (1957).

<sup>15</sup> E. Beltrametti and G. Tomasini, *Nuovo cimento* **18**, 688 (1960).

<sup>16</sup> T. Gooding and H. Pugh, *Nuclear Phys.* **18**, 46 (1960); K. Riley, *Nuclear Phys.* **13**, 407 (1959); K. Riley, T. Gooding, and H. Pugh, *ibid.* **18**, 65 (1960); T. Gooding and H. Pugh, *J. phys. radium* **21**, 326 (1960).

<sup>17</sup> K. Greider, *Phys. Rev.* **114**, 786 (1959).

<sup>18</sup> P. Cooper and R. Wilson, *Nuclear Phys.* **15**, 373 (1960).

difference has been explained<sup>19</sup> as being due to short-range correlations existing in real nuclear wave functions but lacking in independent particle wave functions. These correlations, which are due to the residual two-body interactions, e.g., the repulsive core, etc., produce more high-momentum components in the single-nucleon wave function than does a smooth shell-model potential.

In this work we shall show that the difference between the real nucleon momentum distribution and that given by the shell model is not as great as the experimental results would seem to indicate. Our work will be based on the ideas advanced by McCarthy *et al.*<sup>20</sup>: that the refraction and localization effects caused by the real and imaginary parts of the optical potential contribute enough high-momentum components to explain much and possibly all of the difference between the shell-model and the experimental results. Almost all the experimental work to date has neglected this important effect entirely, or included the optical potential distortion effects in such a manner as to discard most of the localization and refractions. Consequently, the lack of high-momentum components had to be made up in the nucleon-momentum distribution.

In Sec. II, we shall present a brief review of some of the experimental work done to date. The ideas of McCarthy *et al.*<sup>20</sup> will be discussed and extended in Sec. III. In particular, we shall suggest that it appears impossible to measure *directly* by any means, the nuclear momentum distribution. We shall also see that the reaction matrix element contains the Fourier transform of a "wave function" which is the product of distortion factors and a nuclear overlap or single-particle wave function. In Sec. IV, we shall make specific calculations for the  $(p,d)$  reaction to support the contentions of this work. In order to evaluate the distorted wave integrals analytically, we shall make some approximations which do not, in contradistinction to earlier work,<sup>17</sup> discard much of the localization and refraction effects. The results of our calculations are discussed in Secs. V and VI.

## II. EARLIER WORK

The results of 155–925 MeV<sup>1-7</sup> proton-nucleus quasi-elastic and inelastic scattering experiments were analyzed in the plane-wave Born or impulse approximation with several functional forms for the momentum distribution, such as the degenerate Fermi gas form,<sup>1</sup> the one-<sup>2-4</sup> or two-<sup>5</sup> component Gaussian distribution, and the harmonic oscillator<sup>6,7</sup>  $1s$ - and  $1p$ -shell distri-

butions. The results show roughly that for a one-component Gaussian dependence,  $\exp(-E/E_0)$ ,  $E_0 \approx 16$  to 20 MeV, and for a two-component Gaussian,  $\exp(-E/E_1) + b \exp(-E/E_2)$ ,  $E_1 = 7$  MeV,  $E_2 = 40$  MeV, and  $b = 0.05$ . For the  $1s$  and  $1p$  oscillator functions for  $C^{12}$ ,  $\exp(-E/E_s)$  and  $(E/E_p) \exp(-E/E_p)$ , respectively,  $E_s$  and  $E_p$  were found to be 16 MeV and 6–7 MeV,<sup>6,7</sup> respectively.

Similar Born approximation analyses of meson production by 340–380 MeV protons<sup>8,9</sup> or high-energy bremsstrahlung<sup>10</sup> were made using the one-component Gaussian and the Chew-Goldberger distribution,<sup>11</sup>  $a/[\pi^2(a^2 + p^2)^2]$ . The results obtained are roughly the same as those given above, i.e.,  $E_0 = 13$  MeV<sup>8,9</sup> and  $a^2$  corresponds to an energy of 18 MeV.<sup>10</sup> A study<sup>12</sup> of the  $(\gamma, np)$  reaction using 340-MeV bremsstrahlung on the targets Li, C, and O gave  $E_0 = 8$  MeV for Li and  $E_0 = 19$  MeV for C and O with the one-component Gaussian. The pickup reaction induced by 90–120 MeV nucleons<sup>11,13-15</sup> has been similarly analyzed using the Born approximation. For the Chew-Goldberger distribution<sup>11,15</sup>  $a^2$  corresponds to 18 MeV and for the one-<sup>14</sup> and two-<sup>13</sup> component Gaussian it was found that  $E_0 = 16$  MeV and  $E_1 = 7$  MeV,  $E_2 = 50$  MeV, and  $b = 0.15$ , respectively.

Except for normalization, all the results quoted above have neglected any effect of the nuclear optical potential. The nucleus has been assumed to be perfectly transparent to the incident and outgoing particles. There have also been some studies of the above types of nuclear reactions made with the distortion of the particle waves by the optical potential calculated in various approximations.

Using a linear WKB approximation, Riley, Gooding, and Pugh<sup>16</sup> have calculated the distortion effects for the  $(p, 2p)$  reaction at 153 MeV with the harmonic oscillator (H.O.)  $1p$ -shell wave function of  $C^{12}$  and a spring constant obtained from electron scattering results of  $E_p \approx 7$  MeV. They compared the angular distribution so obtained, with that of the Born approximation and with experimental results, and found that the distorted-wave calculations give better agreement with experiment than the Born approximation by filling in the minima. They do not discuss the sensitivity of these results to the target nucleon momentum distribution. However, they do show that in the Born approximation the results are insensitive to the momentum distribution of the struck nucleon. Finally, Greider<sup>17</sup> has shown that if one makes a simplifying approximation to a WKB calculation of the distortion of the incident and exit waves, the 95-MeV<sup>13</sup> and 145-MeV<sup>18</sup>  $C^{12}(p,d)C^{11}$  differential cross sections can be fit with a one-component Gaussian momentum distribution with  $E_0 = 14$  MeV. He points out that his distorted-wave calculations do not require the presence of the high-momentum components,  $E_2 = 50$  MeV, which were needed in earlier work.<sup>13</sup>

From these results one can conclude that, as a rough

<sup>19</sup> K. Brueckner, R. Eden, and N. Francis, *Phys. Rev.* **98**, 1445 (1955).

<sup>20</sup> R. Eisberg, I. McCarthy, and R. Spurrier, *Nuclear Phys.* **10**, 571 (1959); I. McCarthy, *ibid.* **10**, 583 (1959); **11**, 574 (1959); I. McCarthy, E. Jezak, and A. Krominga, *ibid.* **12**, 274 (1959); G. Baker, I. McCarthy, and C. Porter, *Phys. Rev.* **120**, 254 (1960); I. McCarthy and D. Pursey, *ibid.* **122**, 578 (1961); A. Krominga and I. McCarthy, *Phys. Rev. Letters* **4**, 288 (1960).

average the *effective* momentum distribution of nucleons in light nuclei can be represented by a one-component Gaussian distribution with  $E_0$  between 13 and 20 MeV. By an effective distribution, we mean one which includes both the real distribution and the distortion effects. The  $(p,2p)$  data indicate relative insensitivity<sup>3,6,7,16</sup> to the nuclear momentum distribution in that it can fit with H.O. or Gaussian distributions with  $E_0$  (or  $E_s$  and  $E_p$ ) ranging from 7 to 20 MeV or more. The electron scattering results<sup>21</sup> give for the  $C^{12}$   $1p$  shell a value of  $E_p$  of 7.4 MeV in the distribution function,  $(E/E_p) \exp(-E/E_p)$ . We see that for large values of  $E$  this distribution has a smaller amount of high-momentum components than  $\exp(-E/E_0)$  with  $E_0 = 13-20$  MeV.

### III. THE EFFECT OF THE OPTICAL POTENTIAL

In a series of papers McCarthy *et al.*<sup>20</sup> have discussed the distortion effect of the optical potential on the particle waves initiating and emerging from nuclear reactions. They have separated the distortion effects into the phase and amplitude distortion caused by the real and imaginary parts of the optical potential. The phase distortion essentially focuses the particles by refractive effects. The strength of the focusing decreases as the particle energy increases,<sup>20</sup> but is still appreciable at energies around 100 MeV. The amplitude distortion produces a spatial localization of the nuclear reaction sites to some preferred region (e.g., the surface) of the nucleus. This localization is caused by the absorption of the particles from the incident and exit waves into different reactions than the one under consideration.

McCarthy *et al.*<sup>20</sup> observe that, because of this localization, the uncertainty principle requires that the momentum distribution of the outgoing particles be smeared. As they point out, the distribution especially of high components of the momentum of the outgoing particles is more dependent on the momentum components of the localization or distortion than on any components in a target nucleon wave function, which is localized only to within the nucleus. They also discuss the separation of the localization into radial and angular parts and point out that if there is any angular localization, e.g., localization to some parts of the surface region, then the angular momentum resolution is smeared or equivalently, the distortion carries angular momentum. The equatorial localization already found<sup>20,22</sup> for simple reactions consequently carries both radial and angular momentum components.

We would like, in this work, to amplify and extend these ideas to the general problem of determining the momentum distribution of nucleons in the nucleus.

First of all, we would like to suggest that it appears impossible to measure *directly*, by any means, the momentum distribution of a nucleon in the target nucleus. This is based on the fact that the two- (or more-) body interaction which describes the reaction of the probe with a nucleon is the same interaction which describes the probe's reaction with the rest of the nucleus, the elastic part of which is the complex optical potential.<sup>23</sup> The optical potential will be zero in only two cases. Either the two-body interaction is equal to zero or it is such as to give zero-valued diagonal matrix elements between states of the target nucleus. If the two-body interaction is equal to zero, the momentum distribution is unobservable as the reaction cross section is equal to zero. For all types of probe-nucleus interactions found so far, the diagonal matrix elements are different from zero, i.e., there is an optical potential<sup>23</sup> for a probe-nucleus system whenever there is a probe-nucleon interaction. There is also an optical potential for any particle emitted by the probe-nucleon interaction(s).

Even though the nucleon momentum distribution is not directly measured, we do measure a related quantity, the distorted momentum distribution. This distribution is essentially the Fourier transform of a "wave function" which is a product of the single-particle wave function and the distortion factors. Since the value of the distortion factors is a maximum in some restricted region of the nucleus, the product wave function is more localized than the single-particle function and contains more high-momentum components. For simple direct nuclear reactions at energies of 100 MeV the region of preferred reaction sites is the equatorial surface region.<sup>20</sup> Roughly, this same localization is also quite pronounced in the multi-BeV region,<sup>22</sup> due mainly to meson production and should also influence the momentum distribution of secondaries produced in cosmic-ray jets.

Perhaps we can make these ideas more explicit by considering a general transition matrix element for a reaction in which one target nucleon is removed from the nucleus by some type of direct interaction. The transition matrix element is

$$M_{if} = \langle \psi_0^-(\mathbf{r}_0) \psi_1^-(\mathbf{r}_1) \varphi_{\text{int}}(\mathbf{r}_0 - \mathbf{r}_1) \Psi_f(\boldsymbol{\tau}_{A-1}) \rangle \\ \times | I(\mathbf{r}_0 - \mathbf{r}_1) | \psi_0^+(\mathbf{r}_0) \Psi_i(\boldsymbol{\tau}_{A-1}, \mathbf{r}_1) \rangle, \quad (1)$$

where we have suppressed inessential spin and exchange contributions. We have limited ourselves here to one incoming particle, denoted by the distorted wave function  $\psi_0^+(\mathbf{r}_0)$  and two outgoing particles denoted by similar wave functions  $\psi_0^-(\mathbf{r}_0)$ ,  $\psi_1^-(\mathbf{r}_1)$ , as well as one internal wave function,  $\varphi_{\text{int}}(\mathbf{r}_0 - \mathbf{r}_1)$ , between particles 0 and 1. These limitations are not essential to the argument here; we could have many nucleons and mesons, each described by distorted waves, coming out

<sup>21</sup> H. Ehrenberg, R. Hofstadter, U. Meyer-Berkhout, D. Ravenhall, and S. Sobotka, *Phys. Rev.* **113**, 666 (1959).

<sup>22</sup> P. Benioff, *Phys. Rev.* **119**, 324 (1960): Here the distortion effects including the target nucleon spatial distribution are computed directly for the total  $(p,pn)$  or  $(p,2p)$  cross section using a purely imaginary optical potential.

<sup>23</sup> H. Feshbach, *Ann. Rev. Nuclear Sci.* **8**, 49 (1958); A. Kerman, H. McManus, and R. Thaler, *Ann. Phys. (New York)* **8**, 551 (1959); A. Glassgold, *Revs. Modern Phys.* **30**, 419 (1958).

of the target nucleus. The initial and final nuclear state wave functions are denoted by  $\Psi_i$  and  $\Psi_f$ , respectively, and  $I(\mathbf{r}_0-\mathbf{r}_1)$  is an appropriate two-body interaction.

We shall define distortion factors  $D^\pm(\mathbf{r}_i)$  by requiring that

$$\psi^\pm(\mathbf{r}_i) = D^\pm(\mathbf{r}_i)e^{i\mathbf{k}_i \cdot \mathbf{r}_i}, \quad (2)$$

where  $D$  contains all the distortion effects. We now assume that  $I(\mathbf{r}_0-\mathbf{r}_1)$  is of sufficiently short range so that the distortion factors,  $D$ , which typically vary appreciably over distances of the order of nuclear radii, don't change much over the range of  $I(\mathbf{r}_0-\mathbf{r}_1)$  for which  $I \neq 0$ . Using this simplifying but inessential restriction,<sup>20,24</sup> we can factor the matrix element to give (we have let  $\mathbf{r}_0 = \mathbf{r}_1 + \mathbf{r}$ )

$$M_{if} = \langle e^{i\mathbf{q} \cdot \mathbf{r}_1} D_1^-(\mathbf{r}_1) D_2^-(\mathbf{r}_1) | \theta_{if}(\mathbf{r}_1) D_1^+(\mathbf{r}_1) \rangle \times \langle e^{i\mathbf{k}_1 \cdot \mathbf{r}} \varphi_{\text{int}}(\mathbf{r}) | I(\mathbf{r}) | e^{i\mathbf{k}_0 \cdot \mathbf{r}} \rangle. \quad (3)$$

The nuclear wave function overlap is defined by

$$\theta_{if}(\mathbf{r}_1) = \int \Psi_f^*(\boldsymbol{\tau}_{A-1}) \Psi_i(\boldsymbol{\tau}_{A-1}, \mathbf{r}_1) d\boldsymbol{\tau}_{A-1}. \quad (4)$$

If recoil effects are neglected we have, for  $(p,d)$  reactions,  $D_1^-(\mathbf{r}_1) = 1$  and  $\mathbf{q} = \mathbf{K} - \mathbf{k}_0$ ,  $k_1 = \mathbf{K}/2$ ; and for  $(p,2p)$  or  $(p,pn)$  reactions,  $\varphi_{\text{int}}(\mathbf{r}) \simeq 1$  and  $\mathbf{q} = \mathbf{k}_1 + \mathbf{k}_2 - \mathbf{k}_0$ , where  $\mathbf{k}_0$  is the incident nucleon momentum and  $\mathbf{K}$ ,  $\mathbf{k}_1$ , and  $\mathbf{k}_2$  are the respective outgoing deuteron and nucleon momenta. The vector,  $\mathbf{q}$ , is the quantity which is varied in  $(p,d)$  or  $(p,2p)$  differential cross section measurements. The main result is given by Eq. (3), where we see that the transition matrix element is proportional to the amplitude for finding the momentum  $\mathbf{q}$  in the "single-particle wave function,"  $D(\mathbf{r}_1)\theta(\mathbf{r}_1)$ . For brevity all the distortion factors are lumped into one  $D(\mathbf{r}_1)$ .

We can now understand the origin of the high-momentum components. The function,  $\theta(\mathbf{r}_1)$ , often taken to be a shell-model wave function, localizes the target nucleon to be somewhere in the nucleus. The function  $D(\mathbf{r}_1)\theta(\mathbf{r}_1)$  effectively localizes the target nucleon to some restricted region of the nucleus, e.g., the equatorial surface region, and, by the uncertainty principle, has more high-momentum components than does  $\theta(\mathbf{r}_1)$ . It should be understood that  $D(\mathbf{r}_1)$  does not actually localize the target nucleon to some region but instead describes the regions of preferred sampling of the target nucleon wave function. That part of  $D(\mathbf{r}_1)$  coming from the real part of the optical potential, while not localizing the sampled regions, distorts the phase relations of the different parts of the incident and exit waves and effectively alters the momentum distribution. In the Born approximation  $D(\mathbf{r}_1) = 1$  and we have the familiar result that  $M$  is proportional to the amplitude for finding momentum,  $\mathbf{q}$ , in the overlap function,  $\theta(\mathbf{r}_1)$ .

If we write the distortion containing part of  $M$  in the momentum representation we find, as McCarthy *et al.*<sup>20</sup> do, that

$$M \propto \int \hat{p}(\mathbf{k}' - \mathbf{q}) N(\mathbf{k}') d\mathbf{k}'. \quad (5)$$

Here  $N(\mathbf{k}')$  is the amplitude for finding momentum  $\mathbf{k}'$  in the nuclear overlap function. The factor  $\hat{p}(\mathbf{k}' - \mathbf{q})$  denotes the amplitude for finding the momentum  $\mathbf{k}' - \mathbf{q}$  in the distortion factors. We see that we can have a small value of  $\mathbf{k}'$  yet have an appreciable amplitude for producing a large  $\mathbf{q}$  if  $\hat{p}(\mathbf{k}' - \mathbf{q})$  has a broad enough momentum distribution. Equation (5) is our main justification for asserting the impossibility of directly measuring the distribution of  $\mathbf{k}'$  as we see that we must integrate over  $\mathbf{k}'$  in the matrix element, not in the square of the matrix element. Only if  $\hat{p}(\mathbf{k}' - \mathbf{q}) = \delta(\mathbf{k}' - \mathbf{q})$ , as it is in the Born approximation, could one measure directly the momentum distribution of the nuclear overlap wave function.

From this discussion, we see that any approximations made in the calculation of the distortion factors must roughly reproduce the correct spatial localization and refraction if the result is to be used to study the momentum components of the overlap function. If the approximate form of  $D(\mathbf{r}_1)$  contains too little (much) localization and refraction then the experimental analysis will yield too many (few) high-momentum components in the overlap function.

#### IV. THE $(p,d)$ REACTION

For the remainder of this paper, we shall apply these ideas to the  $(p,d)$  reaction. The experimental data in the literature for this reaction are better suited than those of the  $(p,2p)$  reaction<sup>6,7,16,25</sup> to study the momentum distribution of target nucleons. This is due to the fact that most of the  $(p,2p)$  data were not taken at angles corresponding to a large momentum of the target nucleon.

##### A. Theory

The distorted-wave Born approximation matrix element is obtained from Eq. (1) by replacing both outgoing nucleon wave functions by one for the deuteron center of mass. The matrix element is<sup>17</sup>

$$M_{if} = \langle \psi_D^-(\mathbf{R}) \varphi(\mathbf{r}_0 - \mathbf{r}_1) \Psi_f(\boldsymbol{\tau}_{A-1}) \rangle \times \langle V(\mathbf{r}_0 - \mathbf{r}_1) | \psi_0^+(\mathbf{r}_0) \Psi_i(\boldsymbol{\tau}_{A-1}, \mathbf{r}_1) \rangle, \quad (6)$$

where  $\mathbf{R} = (\mathbf{r}_0 + \mathbf{r}_1)/2$ ,  $\Psi_i$  and  $\Psi_f$  are the wave functions as defined for Eq. (1), and  $V(\mathbf{r}_0 - \mathbf{r}_1)$  is the neutron-proton triplet potential.<sup>11</sup> We now follow the previous development of Eqs. (1)-(4) and factor the above matrix element<sup>11</sup> to obtain

$$M_{if} = \langle e^{i\mathbf{q} \cdot \mathbf{r}_1} D_D^-(\mathbf{r}_1) | D_p^+(\mathbf{r}_1) \theta_{if}(\mathbf{r}_1) \rangle \times \langle \varphi_{\text{int}}(\mathbf{r}) | V(\mathbf{r}) | e^{i\mathbf{p} \cdot \mathbf{r}} \rangle \quad (7)$$

<sup>24</sup> N. Austern, Ann. Phys. (New York) **15**, 299 (1961).

<sup>25</sup> N. Bessis, Compt. rend. **248**, 2168 (1959).

where

$$\mathbf{q} = [A/(A-1)]\mathbf{K} - \mathbf{k}_0, \quad (8)$$

and

$$\mathbf{p} = \mathbf{k}_0 - \frac{1}{2}\mathbf{K}. \quad (9)$$

The factor,  $A/(A-1)$ , is introduced to take account of nuclear recoil.<sup>26</sup> The vectors  $\mathbf{k}_0$  and  $\mathbf{K}$  denote the c.m. proton and deuteron momenta, respectively. To obtain Eq. (7) we have replaced  $\mathbf{r}_0$  by  $\mathbf{r} + \mathbf{r}_1$  and defined  $\psi_{D^-}(\mathbf{R})$  by

$$\psi_{D^-}(\mathbf{R}) = D_{D^-}(\mathbf{R})e^{i\mathbf{K}\cdot\mathbf{R}}. \quad (10)$$

The c.m. differential cross section is given by<sup>17</sup>

$$\frac{d\sigma}{d\Omega} = \frac{3}{4} \frac{m^2 A (A-1)}{2\pi^2 \hbar^2 (A+1)^2 k_0} \sum_f K_f |M_{if}|^2, \quad (11)$$

where  $k_0$  is the proton c.m. momentum and the factor  $3/4$  is the spin statistical weight factor. The deuteron momentum,  $K_f$ , is determined by energy conservation to be<sup>13</sup>

$$K_f = \left[ \frac{4(A-1)m}{(A+1)\hbar^2} \left( \frac{A}{A+1} E_L + Q_f \right) \right]^{1/2}. \quad (12)$$

The laboratory system incident kinetic energy is  $E_L$ ,  $A$  is the target atomic weight,  $m$  is the nucleon mass, and  $Q_f$  is the mass difference between the initial and final states ( $Q_f < 0$  for endothermic reactions). We shall take  $C^{12}$  to be the target nucleus. For a  $j-j$  coupled spin-zero target nucleus, the final-state sum,  $\sum_f$ , reduces Eq. (11) to

$$\frac{d\sigma}{d\Omega} = \frac{3}{4} \frac{m^2 A (A-1)}{2\pi^2 \hbar^4 (A+1)^2 k_0} \left[ K_{1s} N_{1s} |M_{1s}|^2 + \frac{K_{1p} N_{1p}}{3} \sum_{m=-1}^1 |M_{1p,m}|^2 \right]. \quad (13)$$

To get this result we have taken the overlap wave function, Eq. (4), to be a single-particle wave function for the  $1s$  shell or  $1p$  shell corresponding to the picked up nucleon being in a  $1s$  state,  $|M_{1s}|^2$ , or in any one of the three orbital  $1p$  states,  $|M_{1p,m}|^2$ . The sum on  $m$  is over the squares of the matrix element because, for given values of the spin projection of the incident proton, the exit deuteron, and the target nucleus, only one value of  $m$  is possible for a closed shell target nucleus.  $N_{1s}$  and  $N_{1p}$  are the number of  $1s$  and  $1p$  neutrons in  $C^{12}$ : We shall leave them as normalizing parameters when comparing theory to experiment. This is the only use we shall make here of spins as we shall in the following neglect any spin-orbit terms in the optical potential.

<sup>26</sup> This result can be derived by making a change of variable in Eq. (6) to the c.m. system of the target nucleus and relative coordinates and integrating over the resultant momentum conservation delta function,  $\delta(\mathbf{K}' + \mathbf{K})$ , for the total c.m. system. The nuclear recoil is denoted by  $\mathbf{K}'$ .

## B. Matrix Element Evaluation

If we choose a Hulthén wave function for the deuteron, then the right-hand matrix element of Eq. (7) can be taken directly from the literature.<sup>11,17</sup> It is

$$\langle \varphi_{\text{int}}(\mathbf{r}) | V(\mathbf{r}) | e^{i\mathbf{p}\cdot\mathbf{r}} \rangle = \frac{4\pi B \hbar^2}{m} \left( \frac{\gamma^2 - \epsilon^2}{\epsilon^2} \right) \frac{1}{1 + \mathbf{p}^2/\epsilon^2}, \quad (14)$$

with

$$B = \left[ \frac{\gamma \epsilon (\gamma + \epsilon)}{2\pi (\epsilon - \gamma)^2} \right]^{1/2}. \quad (15)$$

The factor  $\gamma$  is given by  $\gamma = (mB_D/\hbar^2)^{1/2}$ , where  $B_D$  is the deuteron binding energy and  $\epsilon = 6.2\gamma$ .

The remaining matrix element is a bit more complicated. Our method of evaluation has some points in common with that given by Squires.<sup>27</sup> The two distortion functions,  $D_p^+(\mathbf{r}_1)$  and  $D_{D^-}(\mathbf{r}_1)$  are given by line integrals through the optical potential along the incident proton and exit deuteron momentum vectors respectively,<sup>28</sup>

$$D_p^+(\mathbf{r}_1) = \exp \left[ \frac{-iE_{pL}}{k_{0L}\hbar^2 c^2} \int_{-\infty}^z V_p(\mathbf{r}_1) dz \right], \quad (16)$$

$$D_{D^-}(\mathbf{r}_1) = \exp \left[ \frac{-iE_{DL}}{K_L \hbar^2 c^2} \int_z^{\infty} V_D(\mathbf{r}_1) dz_{KL} \right], \quad (17)$$

where  $E$  is the total lab energy of the particle, including the rest mass. The proton and deuteron optical potentials are given by  $V_p(\mathbf{r}_1)$  and  $V_D(\mathbf{r}_1)$ . The proton is incident parallel to the  $z$  axis from  $-\infty$ . The integral  $\int_{-\infty}^{\infty} dz_{KL}$  is along the direction of  $\mathbf{K}_L$  from the point at which the deuteron is produced to  $+\infty$ . The derivation of these expressions has been given many times before.<sup>27,28</sup> We merely remark here that these expressions are the result of the substitution of Eqs. (2), after they are transformed into the lab system [ $\mathbf{k}_0 \rightarrow (A+1)\mathbf{k}_0/A = \mathbf{k}_{0L}$  and  $\mathbf{K} \rightarrow \mathbf{K} + \mathbf{k}_0/A = \mathbf{K}_L$ ] into the one-body Klein-Gordon (or Schrödinger) equations. The equations are solved by essentially the linear WKB method, i.e.,  $\nabla^2 D$  is neglected in comparison to  $kdD/dz$ .

It is worth noting that  $D_{D^-}(\mathbf{r}_1)$  is the complex conjugate of the time-reversed solution and, in the derivation of Eq. (17), one must be careful with the signs and ordering of the integration limits. One way to evaluate  $D_{D^-}(\mathbf{r}_1)$  is to determine  $D_{D^+}(\mathbf{r}_1)$  in the actual reversed scattering in which the deuteron is incident along  $-\mathbf{K}$ , and then use the relation,<sup>29</sup>  $D_{D^+}(-\mathbf{K}, \mathbf{r}_1) = D_{D^-}(\mathbf{K}, \mathbf{r}_1)$ .

<sup>27</sup> E. Squires, *Nuclear Phys.* **6**, 504 (1958).

<sup>28</sup> R. Glauber, *Lectures in Theoretical Physics* (Interscience Publishers, Inc., New York), Vol. I; L. Schiff, *Phys. Rev.* **103**, 443 (1956); G. McCauley and G. Brown, *Proc. Phys. Soc. (London)* **71**, 893 (1958); S. Brenner and G. Brown (unpublished notes).

<sup>29</sup> E. Merzbacher, *Quantum Mechanics* (John Wiley & Sons, Inc., New York, 1961), Chap. 21, pp. 500, 501.

For actual calculations two approximations will be made. First we shall use  $D_D^{-*}(\mathbf{r}_1)$  computed for forward scattering ( $\mathbf{K}$  parallel to  $\mathbf{k}_0$ ) for all directions of  $\mathbf{K}$ . This approximation, which has been used in other work,<sup>22,27</sup> is exact for forward scattering and should contribute appreciable errors only for large scattering angles where the actual path lengths are different from the forward scattering path lengths. The other approximation consists of the replacement of the expression  $D_D^{-*}(\mathbf{r}_1)D_p^+(\mathbf{r}_1)$  appearing in the matrix element of Eq. (9) by the expression

$$\exp\left(-i\int_{-\infty}^{\infty} N(\mathbf{r}_1)dz\right). \tag{18}$$

We take  $N(\mathbf{r}_1)$  to be an arithmetic average of  $E_{pL}V_p(\mathbf{r}_1)/(k_{0L}\hbar^2c^2)$  and  $E_{DL}V_D(\mathbf{r}_1)/(K_L\hbar^2c^2)$ , where  $V_p(\mathbf{r}_1)$  and  $V_D(\mathbf{r}_1)$  are taken as spherically symmetric potentials with the same radial dependence but different central values. Use of Eq. (18) will allow us to analytically integrate the distortion containing matrix element for  $M_{if}$  as a simple power series.

Using these approximations, we get for the distortion containing part of  $M_{if}$

$$B_{if} = \int e^{-i\mathbf{q}\cdot\mathbf{r}_1} \exp\left[-i\int_{-\infty}^{\infty} N(\mathbf{r}_1)dz\right] \times R_{nlj}(\mathbf{r}_1)Y_{lm}(\theta, \varphi)d\mathbf{r}_1, \tag{19}$$

where  $\theta_{if}(\mathbf{r}_1)$  has been replaced by a single-particle wave function with  $R_{nlj}$  and  $Y_{lm}$  being, respectively, the radial part and the spherical harmonic. For the target,  $C^{12}$ , the radial dependence of  $V_p(r)$ ,  $V_D(r)$ , and hence  $N(r)$  will be taken as the harmonic oscillator model total nuclear density distribution with one nucleon removed from the  $n, l, j$  shell. This exclusion of the struck nucleon from the optical potential was found to be necessary in other work<sup>30</sup> describing bound-state inelastic scattering on  $C^{12}$ . We shall determine the spring constant,  $\beta'$ , in  $N(\mathbf{r}_1)$  by empirically fitting  $N(\mathbf{r}_1)$  to the experimentally determined Woods-Saxon potential. We then get for  $N(\mathbf{r}_1)$

$$N(\mathbf{r}_1) = N(0)[1 + (7/6)\beta'^2r_1^2] \exp(-\beta'^2r_1^2), \tag{20}$$

corresponding to the removal of a  $1p$  neutron, and

$$N(\mathbf{r}_1) = N(0)\left(\frac{3}{4} + \frac{4}{3}\beta'^2r_1^2\right) \exp(-\beta'^2r_1^2),$$

corresponding to the removal of a  $1s$  neutron. We shall follow through the derivation for the  $1p$  case and merely give the final results for the  $1s$  case.

Using Eq. (20), we obtain for the distortion-contain-

ing factor in Eq. (19)

$$\exp\left[-i\int_{-\infty}^{\infty} N(\mathbf{r}_1)dz\right] = \exp\left[\alpha_p\left(1 + \frac{14}{19}s^2\right) \exp(-s^2)\right], \tag{21}$$

where  $s = \beta'b$  and  $b$  is the impact parameter. The factor,  $\alpha$ , is given by

$$\alpha_p = -19i\pi^{1/2}N(0)/12\beta', \tag{22}$$

where

$$N(0) = \frac{1}{2}\left(\frac{E_{pL}V_p}{k_{0L}\hbar^2c^2} + \frac{E_{DL}V_D}{K_L\hbar^2c^2}\right). \tag{23}$$

$R_{nlj}(r)$  is the harmonic oscillator wave function ( $n=1$ ),

$$R_{1l} = \frac{\beta^{3/2}}{\pi^{1/4}} \left(\frac{2^{l+2}}{(2l+1)!!}\right)^{1/2} (\beta r)^l \exp(-\beta^2r^2/2), \tag{24}$$

where  $(2l+1)!! \equiv (2l+1)(2l-1)\cdots \times 3 \times 1$ .

The integration of the matrix element, Eq. (19), can be done in cylindrical coordinates if the exponential in Eq. (21) is expanded in a power series. Each term of the series can be integrated analytically if we note the simple form of the spherical harmonics ( $\sin\theta = b/r$  and  $\cos\theta = z/r$ ). We substitute Eqs. (24) and the expansion of (21) in Eq. (19), make a change of variable  $t = \beta'z$  [ $\beta^2r^2 = (t^2 + s^2)\beta^2/\beta'^2$ ] and set

$$\mathbf{q}\cdot\mathbf{r} = q_b b \cos(\varphi_a - \varphi) + q_z z. \tag{25}$$

With some algebra and use of the expressions<sup>31</sup>

$$e^{iz \cos\varphi} = \sum_{m=-\infty}^{\infty} e^{im(\varphi + \frac{1}{2}\pi)} J_m(z),$$

and<sup>32</sup>

$$\int_0^{\infty} J_\nu(at) \exp(-p^2t^2)t^{u-1}dt = \frac{\Gamma(\frac{1}{2}u + \frac{1}{2}v)\Gamma(\frac{1}{2}a/p)^v}{2p^u\Gamma(v+1)} {}_1F_1(\frac{1}{2}u + \frac{1}{2}v; v+1; -a/p)$$

we get an expression which can be written in one form for all possible  $m$  and  $l$  for  $C^{12}$ . The result is

$$B_{1l, m} = (-1)^{(\delta_1, l - \delta_{1, m})} i^{l/2} 2^{(l-|m|+3)/2} \pi^{3/4} e^{im\varphi} \times (f/\delta)^{|m|} (g/\delta)^{l-|m|} \exp(-c^2/2\delta^2) D_{lm}(f), \tag{26}$$

<sup>31</sup> P. Morse and H. Feshbach, *Methods of Theoretical Physics* (McGraw-Hill Book Company, Inc., New York, 1953), Part II, p. 1322.

<sup>32</sup> G. N. Watson, *The Theory of Bessel Functions* (Cambridge University Press, New York, 1952), pp. 393, 394.

<sup>30</sup> C. Levinson and M. Banerjee, *Ann. Phys. (New York)* **2**, 471, 499 (1957); **3**, 67 (1959).

where the distortion effect is given by

$$D_{lm}(f) = \sum_{n=0}^{\infty} \sum_{\gamma=0}^n \frac{\alpha_l^n (2d_l)^\gamma (\gamma+1)^{|m|}}{(n-\gamma)! (2n+\delta^2)^{\gamma+|m|+1}} \\ \times \exp\{nf^2/[\delta^2(2n+\delta^2)]\} \\ \times \phi(-\gamma; |m|+1; f^2/(4n+2\delta^2)). \quad (27)$$

In these expressions  $\phi(a; c; x)$  is the confluent hypergeometric function which, in this case, is an associated Laguerre polynomial,  $d$  for  $l=1$  and  $0$  is  $14/19$  and  $16/17$ , respectively, and  $\delta = \beta/\beta'$  where  $\beta'$  and  $\beta$  are the spring constants for the optical potential and nucleon distributions, respectively. The factors  $f$  and  $g$  are the projections of  $\mathbf{q}/\beta'$  on the plane perpendicular to  $\mathbf{k}_0$  and on  $\mathbf{k}_0$ , respectively, and  $c = |\mathbf{q}|/\beta'$ . From Eq. (8), we see that

$$f = \frac{A}{A-1} \frac{K}{\beta'} \sin\theta, \quad (28)$$

$$g = \frac{A}{A-1} \frac{K}{\beta'} \cos\theta - \frac{k_0}{\beta'}, \quad (29)$$

where  $\theta$  is the deuteron scattering angle. For  $l=1$ ,  $\alpha_p$  is given by Eq. (22) and for  $l=0$ ,  $\alpha_s$  is

$$\alpha_s = -17i\pi^{1/2}N(0)/12\beta'. \quad (30)$$

It is rather remarkable that the expression for  $B_{nlm}$  turns out to be factorable into the product of the momentum transform of the single-particle wave function and the distortion effect in momentum space. This allows us to find directly the effect of the distortion on the single-nucleon wave function momentum transform.

### C. Parameter Choice

We shall, for the most part, take the real and imaginary parts of the deuteron optical potential as parameters to vary to give the best fit to the experimentally observed differential cross sections. The proton Woods-Saxon well parameters taken from the literature<sup>23</sup> are given in Table I. For the Woods-Saxon well shape, we have chosen  $r_0 = 1.25$  F and  $a = 0.60$  F. A good fit of Eq. (20) to these values of  $r_0$  and  $a$  is obtained by choosing

$$\beta' = 0.47 \text{ F}^{-1}. \quad (31)$$

The value of  $\beta$  is obtained from the electron-scattering

TABLE I. Low- $Z$  nuclear optical model parameters.

$r_0$ (Fermis)	$a$ (Fermis)	$V+iW$ (MeV)	Energy (MeV)	Reference
1.3	0.66	$-25-15i$	95	23
1.23	0.49	$-15-18i$	130	23

work.<sup>21</sup> It is found to be

$$\beta = 0.60 \text{ F}^{-1}. \quad (32)$$

In order to facilitate a choice of  $V_D$ , Eqs. (26) and (27) were evaluated to  $\leq 1.4\%$  accuracy on the IBM 704 computer. To obtain this accuracy the upper limit on the  $n$  sum varied from 8 for small scattering angles to 14 for large angles.

### V. RESULTS

The solid lines in Figs. 1 and 2 give the best fits to the experimental points, marked by circles and triangles for<sup>13</sup> 95-MeV and<sup>18</sup> 145-MeV incident protons, respec-

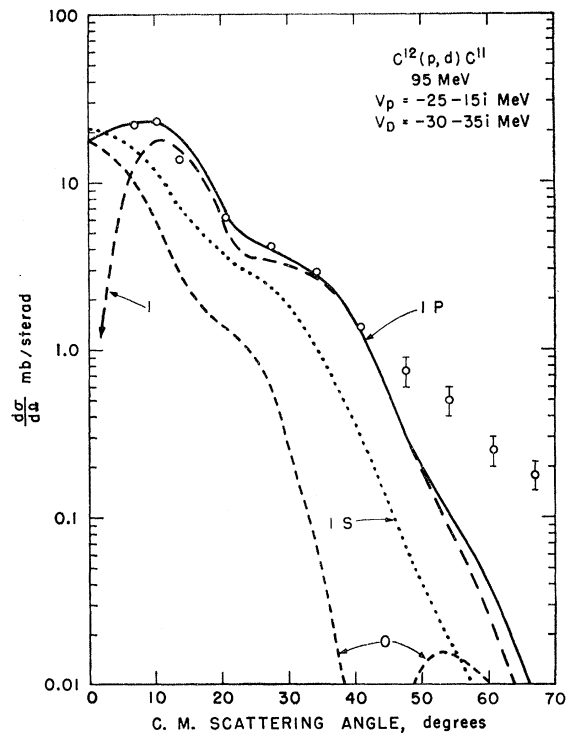


FIG. 1. The  $C^{12}(p,d)C^{11}$  differential cross section for 95-MeV incident protons. The circles, with their associated error limits are the experimental results of Selove. (See reference 13.) The two dashed lines, labeled with 1 and 0, are the partial differential cross sections for  $m = |1|$  and  $m = 0$ , respectively. The solid line is the sum of the  $m = |1|$  and  $m = 0$  curves. The cross section for pickup from the  $1s$  shell is given by the dotted curve.

tively, for the  $1p$  shell pickup reaction in  $C^{12}$ . The two triangles given for each of the larger angles for the 145-MeV data represent two extreme ways of analyzing the experimental data and, as such, give the range in which the correct value should lie. The  $1p$  shell cross section is made up of contributions from neutrons with orbital projection quantum numbers  $m = 1$  and  $0$ . (The contribution for  $m = -1$  equals that for  $m = 1$ .) The dashed lines give these partial cross sections. The curve for  $m = 1$  is multiplied by two to include  $m = -1$ . The dotted line gives the contribution for  $1s$ -shell

neutrons, normalized to half the effective number of  $1p$ -shell neutrons.

The values of the deuteron optical potential which were required to give this best fit are

$$V_D = -30 - 35i \text{ MeV}, \quad E_{\text{proton}} = 95 \text{ MeV}, \quad (33)$$

$$V_D = -30 - 45i \text{ MeV}, \quad E_{\text{proton}} = 145 \text{ MeV}. \quad (34)$$

With these values as well as those given in Table I and Eqs. (31) and (32) the effective number of  $1p$ -shell neutrons required to normalize theory to experiment was found to be 4.0 and 6.7 for 95- and 145-MeV incident energies, respectively. These values are in satisfactory agreement with the expected value of four.

It is of interest to compare the required values of the deuteron optical potential to the values which might be estimated. If we use a suggested simple model<sup>33-35</sup> that the deuteron optical potential equals the sum of the neutron and proton optical potentials taken for nucleons with half the kinetic energy of the deuteron [Eq. (12)], we find for 95-MeV incident protons<sup>23</sup>

$$V_D \sim -(72 + 30i) \text{ MeV},$$

and for 145-MeV protons<sup>23</sup>

$$V_D \sim -(60 + 30i) \text{ MeV}.$$

These crudely estimated potentials have larger real parts and smaller imaginary parts than the potentials of Eqs. (33) and (34). It has been pointed out<sup>35</sup> that, especially for light nuclei, the imaginary part of the deuteron potential should be larger than the sum of the two nucleon imaginary parts. This effect arises from surface stripping. Also the low binding energy of the deuteron should contribute to an increase of the imaginary part of  $V_D$ . On the other hand, the real part of the estimated deuteron potential is larger at both energies than what was required in this work. Other work on elastic scattering of 95-MeV<sup>33</sup> and 167-MeV<sup>34</sup> deuterons on carbon and other nuclei has found the deuteron optical potential to be  $-40 - 20i$  MeV<sup>33</sup> and  $-28 - 16i$  MeV,<sup>34</sup> respectively. Our values for the real and imaginary parts of the deuteron optical potential at both energies are in satisfactory agreement with the above-discussed values when one considers the wide range of the empirical and estimated values.

The ranges of variation of the values of the real and imaginary parts of  $V_D$  which were used to try to fit the experimental data were 15–50 MeV and 10–45 MeV, respectively. We also investigated the effect of changing the extent of the optical potential by varying  $\beta'$ . In general, we needed a large value of the imaginary part and a small value of the real part of  $V_D$  to reproduce

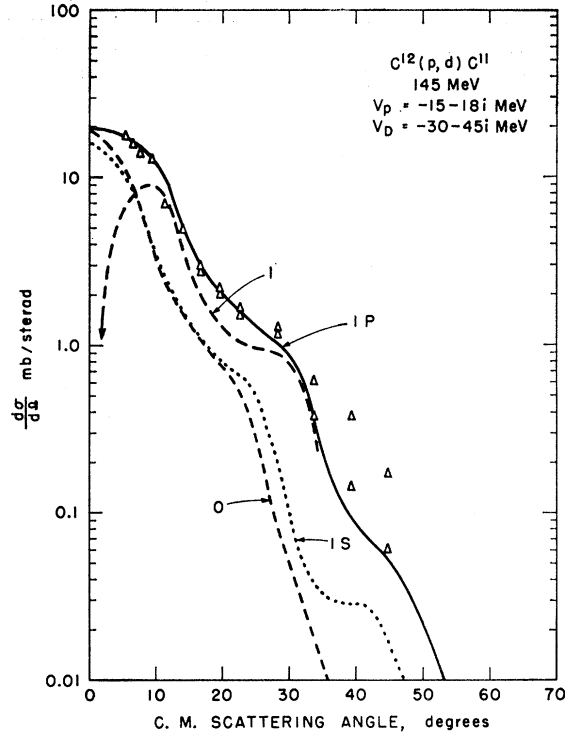


FIG. 2. The  $C^{12}(p,d)C^{11}$  differential cross section for 145-MeV incident protons. The triangles are the experimental data of Cooper and Wilson. (See reference 18.) The double triangles for many points represent two extreme ways of analyzing the data and as such should roughly be the error limits. The two dashed lines, denoted by 1 and 0, are the partial cross sections for  $m = |1|$  and  $m = 0$ , respectively. The solid line is the sum of the  $m = 0$  and  $m = |1|$  curves. The cross section for pickup from the  $1s$  shell is given by the dotted curve.

the dips in curves in Figs. 1 and 2 at  $\sim 20^\circ$ : We were unable to fit the data well with any values of  $V_D$  if  $\beta'$  was appreciably larger than 0.47. For values of  $\beta'$  less than 0.47 we could fit the data but the normalization was less satisfactory and an even larger imaginary part of  $V_D$  was needed.

## VI. DISCUSSION

### A. Momentum Distribution

Perhaps the most important characteristic of the curves in Figs. 1 and 2 is that the experimental data is fitted well for angles smaller than  $35^\circ - 40^\circ$  and for larger angles the calculated curve drops off faster than the experimental results. This lack of agreement at larger angles is most likely due to either an insufficient amount of high-momentum components in the single-particle wave function or the failure of our approximation of using the forward scattering expression for  $D_{D^*}(\mathbf{r})$  for all scattering angles.

We can very crudely estimate which of these factors is most responsible for the lack of agreement at large scattering angles. If it were exclusively our forward-scattering approximation which was causing the dis-

<sup>33</sup> S. Watanabe, Nuclear Phys. 8, 484 (1959).

<sup>34</sup> O. Cheisvilli, J. Exptl. Theoret. Phys. (U.S.S.R.) 32, 1240 (1957) [translation: Soviet Phys.—JETP 5, 1009 (1957)].

<sup>35</sup> H. Melkanoff, Proceedings of the International Conference on the Nuclear Optical Model, Florida State University Studies, No. 32, 1959 (Florida State University, Tallahassee, Florida, 1959), pp. 207–215.

agreement, then one might expect the fractional deviations between theory and experiment to be the same for a given angle at both energies. If the lack of high-momentum components were the cause of error, then the fractional deviation of theory from experiment would be the same for those scattering angles at each energy with the same values of  $c^2/\delta^2 = q^2/\beta^2$  (see Eqs. (26), (27)). These angles can be found from the relative positions of the various "dips and bumps," in Figs. 1 and 2 and are 10–15 deg larger at 95 MeV than at 145 MeV. Examination of Figs. 1 and 2 indicates that the failure of the forward scattering approximation may cause more of the disagreement than the lack of high momentum components in the single-particle wave function. On the whole, the fit of theory to experiment is better at 145 MeV where smaller scattering angles are involved than at 95 MeV. For both sets of data the fit is good for angles  $\leq 35^\circ\text{--}40^\circ$  which corresponds to values of  $q^2/\beta^2 \lesssim 8$ . Recalling that the reaction cross section is the product of the momentum distributions of the distortion and the single-particle wave function, we conclude that  $(q^2/\beta^2) \exp(-q^2/\beta^2)$  contains enough high-momentum components up to  $q^2/\beta^2 \simeq 8$  to reproduce the experimental data. The difference between this distribution and the previously obtained average distribution,  $\exp(-E/E_0)$ , with  $E_0 \sim 13\text{--}20$  MeV ( $q^2/\beta^2 = E/7.5$ ) is appreciable as  $8 \exp(-8) \simeq 0.0027$  but ( $E = 60$  MeV)  $\exp(-E/15) \simeq 0.018$ .

Other approximations made, besides the forward scattering approximation for  $D_D^{-*}(r)$ , are the neglect of the variation of  $D_D^-$  and  $D_p^+$  over the neutron-proton interaction range; Eq. (7), the use of an average value of  $N(r)$ , Eq. (18), and the neglect of changes in the path length in the optical potential due to refraction.<sup>20,23</sup> We feel that the effects of these approximations are smaller than the use of the forward-scattering expression for  $D_D^{-*}(r)$  and can be neglected here.

We conclude, then, that the  $1p$ -shell nucleon momentum distribution fits the harmonic oscillator distribution,  $(q^2/\beta^2) \exp(-q^2/\beta^2)$ , with the spring constant determined from electron-scattering work<sup>21</sup> up to  $q^2/\beta^2 \simeq 8$ . The question of a fit at larger values of  $q^2/\beta^2$ , or the deuteron scattering angle  $> 35^\circ$ , can only be resolved by a more accurate determination of the distortion factors with the correct scattering-angle dependence.

### B. Other Data

The other distorted-wave calculation made to determine nucleon momentum distributions is the work of Greider<sup>17</sup> on the same reaction as was studied here,  $C^{12}(p,d)C^{11}$ . The same experimental data<sup>13,18</sup> as we used was analyzed with a square-well optical potential to give a  $1p$ -shell distribution,  $\exp(-E/14)$ . With this distribution Greider was able to fit the experimental data over the whole range of angles with a normalization of 4–6 neutrons required. He also remarks that one does not need even the high-momentum compo-

nents in  $\exp(-E/14)$  if the incident proton and exit deuteron are allowed to scatter in the nuclear field.

Leaving aside this scattering for the present, we see that there is a large discrepancy between the results of Greider's work, hereafter called I, and our work in that the momentum distribution obtained in I has many more high momentum components than the  $1p$ -shell H.O. distribution obtained in this work. This discrepancy is the result of two factors. One factor, which we feel is the most important, is contained in the equations for the distorted proton and deuteron waves which were actually used in I [Eq. (24) and its equivalent for the outgoing deuteron of reference 17] to evaluate the matrix element. These equations, which contain approximations to the actual path length integrals in a square optical potential  $[(R^2 - r^2 \sin^2\theta)^{1/2} \rightarrow R]$ , essentially replace the spherical nucleus by two cylindrical pieces with end faces perpendicular to the incident proton and outgoing deuteron. This replacement discards most of the refraction and localization effects which a spherical potential has (the refraction and equatorial localization of plane waves incident perpendicular to a cylinder face is essentially zero). As was mentioned at the end of Sec. III this has the consequence that nucleon momentum distributions with too many high-momentum components will be required to fit the experimental data. Thus, we feel that a good portion of the difference between our distribution and  $\exp(-E/14)$  is due to distortion effects which, in I, have been erroneously attributed to the  $1p$ -shell nucleon momentum distributions.

The other factor which helps to account for the discrepancy is that a smaller deuteron optical potential was used in I,  $V_D = -20 - 15i$  MeV, for 95- and 145-MeV incident proton energies, than was used here, Eqs. (33) and (34). The smaller optical potential reduces the distortion by reducing the amount of refraction and localization and consequently supplies less high momentum components. We made calculations at both 95 and 145 MeV using the deuteron and proton optical potentials of I and the values of  $\beta$  and  $\beta'$  given by Eqs. (31) and (32) and got a poor fit to the experimental results even for small scattering angles where our forward scattering approximation for  $D_D^{-*}(r)$  should be good. Also our calculated values of the differential cross section with the potential of I were too large by a factor of 3 requiring an effective  $C^{12}$   $1p$ -shell neutron number of  $4/3$ . Roughly, a correct effective neutron number of 4 to 6 was required in I to fit the experimental data. It can be shown by simple computation that the factor-of-three discrepancy between ours and Greider's<sup>17</sup> calculations is accounted for by the increased path length resulting from the "cylinder approximation used in I. We feel, then, that the deuteron potential,  $-20 - 15i$  MeV, which would give  $4/3$  effective neutrons here and in I and which gives a poor fit in this work to the experimental data, is probably too small.

Because of the approximations used both in I and here, it seems premature to invoke scattering of the proton and deuteron in the nuclear field<sup>17</sup> to explain the presence of any high-momentum components. It could well turn out that, after these approximations have been removed, the data will still show the effects of the initial- and final-state interactions which have been neglected so far.

### C. The Partial Differential Cross Sections

There are some interesting features of the partial differential cross sections shown in Figs. 1 and 2, for picking up neutrons with different orbital projection quantum numbers. First of all, we note the zeros at  $0^\circ$  and  $\sim 42^\circ$  scattering angles for the respective  $m=|1|$  and  $m=0$  partial cross sections. To explain these zeroes, we recall that Eq. (26) is the product of the momentum transform of the single particle wave function,  $\langle e^{i\mathbf{q}\cdot\mathbf{r}} | Y_{lm}(\theta, \varphi) R_{nlj}(r) \rangle$ , and a distortion factor. Since the single-particle momentum transform is proportional to  $Y_{lm}(\theta_q, \varphi_q)$ , the zeroes are those of the spherical harmonics,  $Y_{11} \propto \sin\theta_q$  and  $Y_{10} \propto \cos\theta_q$ , represented by  $f/\delta$  and  $g/\delta$ , respectively, in Eq. (26). The zero for  $Y_{10}$  is at  $42^\circ$  rather than  $90^\circ$ , because  $\theta_q$  refers to the direction of the vector  $\mathbf{q}$  [Eqs. (8), (28), (29)] relative to  $\mathbf{k}_0$  rather than the direction of  $\mathbf{K}$ .

Another feature of the cross sections is that, except for angles of  $\leq 7^\circ$ , the differential cross section and also the integrated cross section consist predominantly of the pickup of the  $m=|1|$  neutron rather than the  $m=0$  neutron. This effect is due to the fact that the distortion effect, especially in the forward-scattering approximation, localizes the region of maximum pickup probability to the nuclear equatorial regions.<sup>20,22</sup> A  $1p$  nucleon with  $m=|1|$  is more likely to be found in the equatorial regions ( $Y_{11} \propto \sin\theta$ ) than a nucleon with  $m=0$  ( $Y_{10} \propto \cos\theta$ ). Consequently, the  $m=|1|$  nucleons contribute more to the cross section than do the  $m=0$  nucleons. This effect and its consequences will be discussed more thoroughly in a subsequent publication.

### D. The Distortion Effect

There are some additional features of the distortion effect, which are worth examining at this point. We have pointed out that the real and imaginary parts of the optical potential distort the incident and exit particle waves by refraction (similar to the bending of light by a spherical lens) and localization, respectively. It is interesting to examine the effects of the real and imaginary parts of the optical potential separate from each other. This is shown in Fig. 3. The solid line marked  $R$  is the 95-MeV differential cross section computed for the same parameters as those used in Fig. 1 except that the imaginary parts of  $V_p$  and  $V_D$  are set equal to zero. Similarly, the solid line marked  $I$  is computed for purely imaginary  $V_p$  and  $V_D$ . The

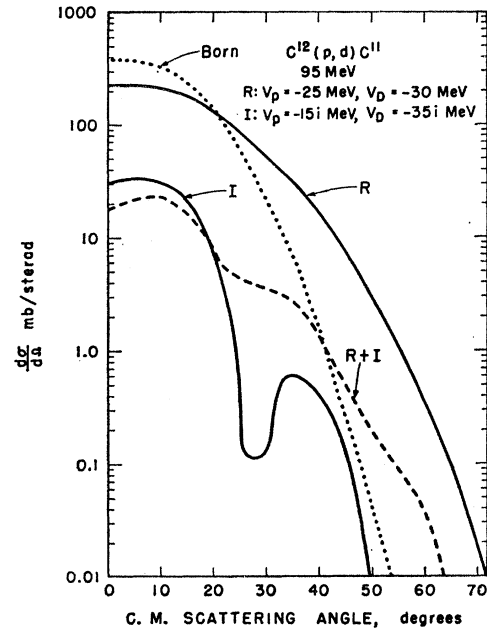


FIG. 3. The 95-MeV  $C^{12}(p, d)C^{11}$   $1p$ -shell differential cross section for special values of the proton and deuteron optical potentials. The solid curves labeled with  $R$  and  $I$  are for pure real and pure imaginary potentials taken from Table I and Eq. (33). The dashed curve is for the complete complex potential and is the solid curve of Fig. 1. The dotted curve is the Born-approximation cross section obtained by setting  $V_p = V_D = 0$ .

dashed line repeats the  $1p$  cross section already given in Fig. 1 and represents the combined effect of the real and imaginary parts of the potential. The dotted line is the Born approximation cross section obtained by setting  $V_p = V_D = 0$ . All the curves are normalized to four  $1p$ -shell neutrons. We notice several characteristics of the curves in Fig. 3. The curve for the real and imaginary parts of the potential are less steep than the Born approximation curve, indicating the addition of high-momentum components by the distortion. The curve for the pure imaginary potential is at least an order of magnitude less than the curve for the pure real potential indicating the large damping effect along the particle paths. We also note an effect which we are at a loss to explain: The purely real potential curve shows no oscillations at all whereas the purely imaginary curve has strong oscillations with minima at  $28^\circ$  and  $\simeq 52^\circ$ . Offhand we might expect the purely real curve to show as much oscillatory behavior as the purely imaginary curve. Finally, we note that the curve of Fig. 1 partakes of both the  $R$  and  $I$  curves: The interference effects are partially washed out, and the general slope of the curve is similar to that of the  $R$  curve.

It is also of interest to examine the distortion factor,  $D_{lm}(f)$  of Eqs. (26) and (27). Figure 4 shows curves of  $|D_{lm}(f)|^2$  as a function of the scattering angle for  $1p$ -shell nucleons with  $m=|1|$  and  $m=0$  for 95-MeV incident protons. The curves of Fig. 4 demonstrate

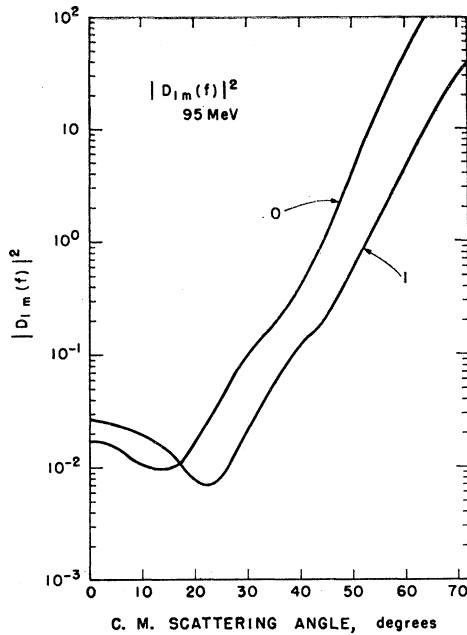


FIG. 4. The  $1p$ -shell distortion factor squared,  $|D_{lm}|^2$  as a function of scattering angle for 95-MeV incident protons. The curves labeled 1 and 0 refer to  $m=|1|$  and  $m=0$ , respectively.

vidently the addition of high-momentum components to the Born approximation cross section; they show an initial flat portion and a dip for small angles and then become essentially an increasing exponential for larger scattering angles [Eq. (27)]. We believe that the reason the distortion effect is larger for  $m=0$  than for  $m=|1|$  is due to the spherical harmonics in the single nucleon wave function. Since  $Y_{1|1|} \propto \sin\theta$  the  $m=|1|$  nucleon is more likely to be in the equatorial rather than the polar regions of the nucleus. As the distortion effect also preferentially selects the equatorial regions, the resultant distorted single-particle wave function is not as different from the undistorted function as it is if  $m=0$ . In this case, as  $Y_{10} \propto \cos\theta$ , the nucleon is preferentially in the polar regions of the nucleus which is the region least likely to contribute to the cross section.

Finally, the strong dependence of the curves of Fig. 4 on the scattering angle show that, in general, it is quite erroneous to assume that the only effect of the distortion is to normalize the cross sections. However, if one confines himself to small values of the effective (real+distortion) target nucleon momentum then the

initial flat portion of the curves show that the main effect of  $|D_{lm}|^2$  is that of normalization. This is why most  $(p,2p)$  quasi-elastic scattering work<sup>16,36</sup> has not found large distortion effects on the momentum distribution.

## VII. CONCLUSIONS

We have analyzed the 95- and 145-MeV  $1p$  shell  $C^{12}(p,d)C^{11}$  differential cross section data in the distorted wave Born approximation. The effect of the distortion was computed with a weighted average potential factor  $N(0)$  in the forward scattering approximation. We found that for  $q^2/\beta^2 \lesssim 8$  with  $\beta$  given by the electron-scattering results, the  $1p$ -shell harmonic oscillator wave function gives sufficient high-momentum components to fit the data for  $\theta \lesssim 35^\circ$ – $40^\circ$  with reasonable values of  $V_D$ . We feel that the lack of agreement between theory and experiment for  $\theta \gtrsim 35^\circ$ – $40^\circ$  may be in large part due to the failure of the forward-scattering approximations rather than lack of high-momentum components in the nuclear wave function. Work is in progress at present to check this point and will be reported in a later publication.

The results obtained here are at variance with the results obtained by other workers<sup>1–15</sup> using the Born approximation or various distorted-wave approximations. We can understand this disagreement in the light of the ideas advanced by McCarthy *et al.*<sup>20</sup> A substantial fraction of the high-momentum components found for target nucleons in nuclei is due to the refraction and localization effects on the incident and exit particle waves caused by the real and imaginary parts of the nuclear optical potential. For this reason, any approximate distorted-wave calculation must correctly reproduce the refraction and localization effects or a nuclear momentum distribution with too many high-momentum components will be obtained.

Finally, we note that for  $q^2/\beta^2$  (or  $E/7.5$ )  $\lesssim 8$  and possibly for  $q^2/\beta^2 \gtrsim 8$  the effects of short-range correlations in adding high-momentum components to the nuclear wave function may be less important than has been assumed.<sup>19</sup>

## ACKNOWLEDGMENT

The author wishes to thank Murray Peshkin for several helpful discussions.

<sup>36</sup> Th. Maris, P. Hillman, and H. Tyrén, *Nuclear Phys.* **7**, 1 (1958); G. Jacob and Th. Maris, *ibid.* **31**, 139 (1962).